Quasiperiodicity and a spin-dependent Kronig-Penney model

1994 J. Phys.: Condens. Matter 6 10283

(http://iopscience.iop.org/0953-8984/6/47/012)

J. Phys.: Condens. Matter 6 (1994) 10283–10296. Printed in the UK

Quasiperiodicity and a spin-dependent Kronig–Penney model

S J Blundell

Clarendon Laboratory, Parks Road, Oxford OX1 3PU, UK

Received 10 August 1994

Abstract. Using a transfer matrix method, the band structure is calculated for a spin-dependent generalization of the Kronig–Penney model which consists of a one-dimensional array of delta function potentials whose strengths depend on the relative orientation of the electron spin and a vector located at each delta function site, the direction of which is helically modulated. This is compared with a spin-independent Kronig–Penney model in which only the amplitude of each delta function is modulated. The period of the modulation can be incommensurate with the periodicity of the delta function array. The fractal nature of the band structure in the spin-independent case is shown to be quenched by the additional symmetry in the spin-dependent model.

1. Introduction

Quasiperiodic systems lie between the extremes of perfect crystalline order and amorphous disorder. These have become of particular interest since the discovery of a quasicrystalline phase (locally exhibiting fivefold symmetry) in metallic alloys [1, 2]. Much theoretical work has been concerned with modelling the transition from periodic to aperiodic order in the 'Fibonacci superlattice' [3, 4, 5, 6] in which the potential energy of an electron at successive sites on a one-dimensional array is positive or negative according to a Fibonacci sequence. Such systems may now have physical realizations in the form of epitaxially grown semiconductor superlattices [7, 8].

Another important example of quasiperiodic systems is the class of *almost periodic crystals* in which the band structure is determined by two periodic functions which are incommensurate with each other [9, 10]. If the ratio between the two periods is rational, the 'unit-cell' size can be much larger than that determined by either of the periodicities acting individually, producing many gaps in the band structure. If the ratio of the two periods is irrational, any periodicity is entirely lost, although it can be formally recovered in higher dimensions [11, 9].

Examples of incommensurate systems include crystals with spin density waves or charge density waves (where the two periods are the lattice spacing and $1/k_F$), and also in certain mercury chain compounds [12] and some organic superconductors [13]. The problem of Bloch electrons on a square lattice in a magnetic field is another example [14, 15] where the two periods are proportional to the flux quantum and the flux through a plaquette.

It is convenient to study quasiperiodicity in all its forms through simple one-dimensional models; tight-binding and Kronig–Penney models have been particularly popular since they admit a simple transfer matrix description. In this paper, a spin-dependent generalization of

0953-8984/94/4710283+14$19.50

the Kronig–Penney model is studied and compared with a corresponding spin-independent model. The fractal nature of the band structure in the spin-independent case is shown to be quenched by the additional symmetry in the spin-dependent model.

The paper is organized as follows: in section 2, a number of introductory remarks are made concerning the approach to modelling quasiperiodic systems; section 3 outlines the application of transfer matrices to the spin-independent Kronig–Penney model; section 4 contains a description of the quasiperiodic modulations which can be made to it and also introduces the transfer matrix solution to the corresponding spin-dependent model; the results are discussed in section 5.

2. Modelling quasiperiodicity in one dimension

An important class of almost-periodic models is based on the discrete Schrödinger equation, describing electrons in the tight-binding approximation, and is given by

$$\hat{H}\psi_j = \mathcal{E}\psi_j = \frac{1}{2}[\psi_{j+1} + \psi_{j-1}] + \lambda\cos(2\pi j\phi + \theta)\psi_j \tag{1}$$

where ψ_j is the wave function at site j, $\mathcal{E}$ is the total energy, θ is some constant phase, λ is a coupling constant, and ϕ controls the frequency of the almost-periodic variation [16]. This is known as the *almost-Mathieu* operator, because of its similarity with the Mathieu operator [17].

An interesting duality has been observed in this system [18]: the discrete Fourier transform of the wave function at each site $\{\psi_j\}$ also satisfies an equation of the same form as equation (1) except that it is necessary to replace λ by $1/\lambda$. Since these two representations of the wave function are Fourier transforms of each other, when a state in one representation is localized, it must be extended in the other. Therefore, when $\lambda = 1$, at the fixed point of this duality transformation, a metal–insulator transition in this model is predicted [18].

The problem of the Bloch electron on a two-dimensional square lattice in a magnetic field, described by the Harper equation [19, 20], is in fact identical to the *almost-Mathieu equation* when $\lambda = 1$. Hence the spectrum of the latter, at $\lambda = 1$, exactly at the 'metal–insulator transition', is a Hofstadter butterfly [20, 21]. At values of λ less than this, the butterfly becomes altered, broadening out until $\lambda = 0$, at which point the potential is 'free-electron-like'—i.e. there are no gaps. The magnetic flux ϕ in units of h/e plays the rôle of the modulation ϕ in the almost-Mathieu equation (equation (1)), which is why they are denoted by the same symbol. Because the spectrum depends on three variables (the energy $\mathcal{E}$, the modulation ϕ, and the modulation strength λ), the entire spectrum can be conveniently visualized with the aid of figure 1 which shows the bands (black) and gaps (white) of a portion of this model. The front face ($\lambda = 1$) of this 'Hofstadter cube' shows part of the Hofstadter butterfly. The 'fractal' structure seen in this model is characteristic of problems which sensitively depend on the value of the integers p and q in the parameter $\phi = p/q$. An extremely simple way in which to observe quasiperiodic behaviour is through the Kronig–Penney model. This has a natural periodicity (determined by the spacing between the delta functions) but an artificial periodicity may be added by modulating the strength of the delta functions with a different periodicity. For example, if the strengths of the delta function potentials in a Kronig–Penney model with period d are sinusoidally modulated with a period md along the y-axis, where m is an integer, then the unit cell grows by a factor m, introducing extra band gaps into the energy spectrum. If m is irrational, the unit cell is effectively infinite in size, and the energy spectrum has infinitely many gaps; it becomes a

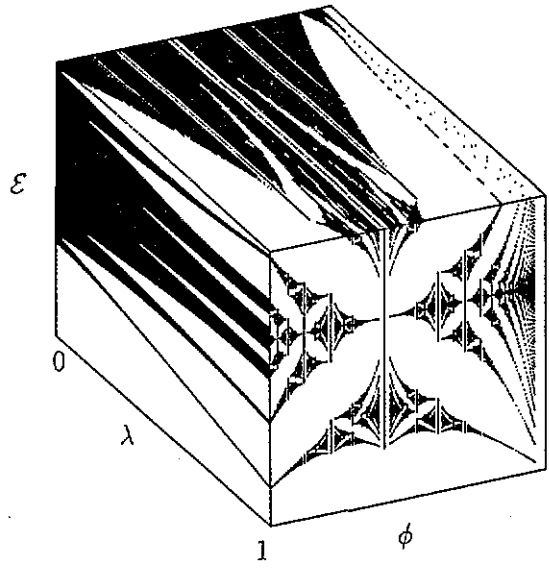

Figure 1. The Hofstadter cube (the spectrum of the almost-Mathieu model). The front face shows a portion of the Hofstadter butterfly ($\lambda = 1$).

Cantor set [9, 16].

It is straightforward to show that the almost-Mathieu equation (1) can be mapped on to the amplitude-modulated (AM) Kronig–Penney model

$$\left[-\frac{d^2}{dy^2} - \sum_{j=-\infty}^{\infty} g\cos(2\pi j\phi + \theta)\,\delta(y - jd)\right]\Psi(y) = E\Psi(y) \tag{2}$$

(where g is the strength of the amplitude modulation, E is the energy, and units are chosen so that $\hbar^2/2m = 1$) by the transformation [22]

$$\mathcal{E} = 2\cos\sqrt{E} \tag{3}$$

$$\lambda = \frac{g}{2}\frac{\sin\sqrt{E}}{\sqrt{E}}. \tag{4}$$

In this way the AM Kronig–Penney model behaves like the almost-Mathieu model with an energy-dependent coupling constant. Using a property of the almost-Mathieu equation, namely that for irrational ϕ (with good diophantine approximation property: i.e., for most irrationals), the spectrum is 'absolutely continuous' for $|\lambda| < 1$, and 'pure point' for $|\lambda| > 1$, it can be shown using equation (4) for which values of g and E the metal–insulator transition occurs in the amplitude-modulated Kronig–Penney model [22].

In the following sections, the transfer matrix method will be used to calculate band structures of spin-independent and spin-dependent Kronig–Penney models which each consist of a one-dimensional array of delta function potentials whose strengths can be modulated in various ways; transfer matrices offer a useful and concise description of one-dimensional quantum mechanical problems [23] and can be used conveniently to demonstrate the analogy between such problems and other electrical, optical, and condensed matter formulations [24]. The Kronig–Penney model is an appropriate choice since it is so

closely related to more general periodic potential barriers and also to tight-binding models (as demonstrated above) [9].

Spin-independent Kronig–Penney models can be calculated using standard 2×2 transfer matrices, but the spin-dependent Kronig–Penney model requires a 4×4 transfer matrix method [25] for its solution. It turns out that this model is quite different from the spin-independent case, in that the quasiperiodicity *no longer* introduces additional gaps into the band structure. The spin dependence of the problem is not important unless the spin of the potential is other than always purely parallel or anti-parallel to some fixed direction. Therefore, I will particularly concentrate on the distribution of bands and gaps in a *helical* magnetization structure.

3. Kronig–Penney model

In figure 2(a), I show a general potential barrier consisting of N regions in each of which the potential $V(y)$ is constant. If the wave function on the left-hand side of the general potential barrier is written as a sum of incident and reflected waves,

$$\psi(y) = e^{ik_1 y} + re^{-ik_1 y} \qquad y < y_1 \tag{5}$$

and the wave function on the right-hand side of the potential barrier is written as a single transmitted wave,

$$\psi(y) = te^{ik_N y} \qquad y > y_{N-1} \tag{6}$$

then it may be shown that [25]

$$\begin{pmatrix} 1 \\ r \end{pmatrix} = \mathbf{D}(k_1)^{-1} \left(\prod_{j=2}^{N-1} \mathbf{D}(k_j)\mathbf{P}(k_j, d_j)\mathbf{D}(k_j)^{-1} \right) \mathbf{D}(k_N) \begin{pmatrix} t \\ 0 \end{pmatrix} \tag{7}$$

where

$$\mathbf{D}(k_j) = \begin{pmatrix} 1 & 1 \\ k_j & -k_j \end{pmatrix} \tag{8}$$

are the matrices which match ψ and $d\psi/dy$ at the interfaces and

$$\mathbf{P}(k_j, d_j) = \begin{pmatrix} e^{-ik_j d_j} & 0 \\ 0 & e^{ik_j d_j} \end{pmatrix} \tag{9}$$

are the propagation matrices. I now consider the case of the Kronig–Penney model which consists of a periodic one-dimensional array of delta function potential barriers spaced a distance d apart along the y-axis, and each with strength g,

$$V(y) = \sum_{j=-\infty}^{\infty} g\,\delta(y - jd). \tag{10}$$

It is convenient to consider a delta function potential barrier as the limit of a rectangular barrier as its height $\kappa^2 + k^2$ grows as $\kappa \to \infty$ and its width ξ shrinks such that $\kappa^2\xi$ is constant (figure 2(b)). Using the transfer matrix method, the amplitude of the forward- and backward-travelling waves at successive delta functions can be related by

$$\begin{pmatrix} a_j \\ b_j \end{pmatrix} = \mathbf{P}(k, d)\mathbf{D}(k)^{-1} \left(\lim_{\substack{\kappa \to \infty \\ \kappa^2\xi = g}} \mathbf{D}(\kappa)\mathbf{P}(\kappa, d)\mathbf{D}(\kappa)^{-1} \right) \mathbf{D}(k) \begin{pmatrix} a_{j+1} \\ b_{j+1} \end{pmatrix}$$

$$= \begin{pmatrix} e^{-ikd} & 0 \\ 0 & e^{ikd} \end{pmatrix} \frac{1}{2} \begin{pmatrix} 1 & 1/k \\ 1 & -1/k \end{pmatrix} \begin{pmatrix} 1 & 0 \\ ig & 1 \end{pmatrix} \begin{pmatrix} 1 & 1 \\ k & -k \end{pmatrix} \begin{pmatrix} a_{j+1} \\ b_{j+1} \end{pmatrix}$$

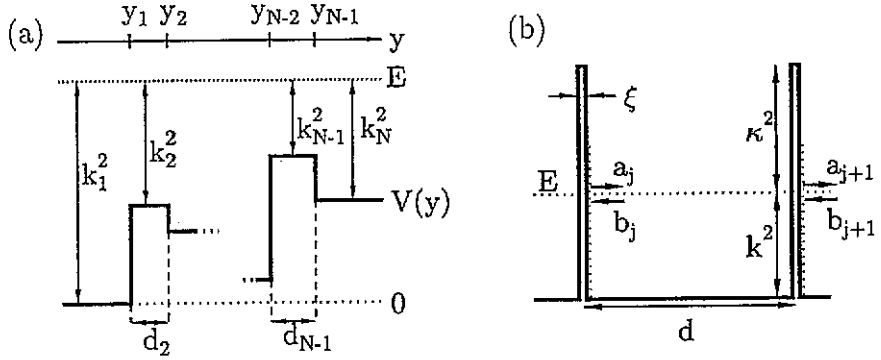

Figure 2. (a) A general one-dimensional potential barrier $V(y)$ composed of N distinct regions in each of which the potential is constant; (b) the Kronig–Penney potential barrier (see text). As $\kappa \to \infty$ with $\kappa^2\xi = g$, the barriers become delta functions with amplitude g. a_j (b_j) is the amplitude of a left- (right-) travelling wave.

$$= \begin{pmatrix} e^{-ikd}(1 + ig/2k) & e^{-ikd}(ig/2k) \\ -e^{ikd}(ig/2k) & e^{ikd}(1 - ig/2k) \end{pmatrix} \begin{pmatrix} a_{j+1} \\ b_{j+1} \end{pmatrix}$$

$$= \mathbf{m}(k, g, d) \begin{pmatrix} a_{j+1} \\ b_{j+1} \end{pmatrix} \tag{11}$$

where a_j and b_j are defined in figure 2(b). To find the bands and gaps in this system, it is necessary to find the eigenvalues of the transfer matrix $\mathbf{m}(k, g, d)$. Because $\det(\mathbf{m}(k, g, d)) = 1$, the product of the two eigenvalues is unity: therefore, if μ is an eigenvalue of $\mathbf{m}(k, g, d)$, so too is $1/\mu$; thus the electrons lie in an allowed band if $|\mu| = 1$. Solutions with $|\mu| \neq 1$ correspond to surface states on a finite chain of the Kronig–Penney lattice and lie in the gaps of the infinite system. Hence an allowed (band) solution is found when $\mathrm{Tr}\,\mathbf{m}(k, g, d)$ (which is equal to the sum of the eigenvalues) is $e^{iqd} + e^{-iqd}$ with q real. (A forbidden (gap) state is found when $\mathrm{Tr}\,\mathbf{m}(k, g, d) = e^{\eta d} + e^{-\eta d}$ with η real). Hence

$$\cos qd = \frac{1}{2}\mathrm{Tr}\,\mathbf{m}(k, g, d) = \cos kd + \frac{g}{2k}\sin kd \tag{12}$$

which is the well known band structure of the Kronig–Penney model. This band structure is characterized by gaps in the spectrum which appear just above (below) each Brillouin zone boundary for positive (negative) g, i.e., for delta function barriers (wells). This band structure is shown in figure 3: the abscissa is $kd/\pi \propto (\text{Energy})^{1/2}$ and the ordinate is gd, measuring the strength of the delta functions. A point is plotted black if it lies within an allowed region (band); it is made white if it lies within a forbidden region (gap). The allowed states (bands) are given by $|\mathrm{Tr}\,\mathbf{m}(k, g, d)| \leqslant 2$.

4. Modulated Kronig–Penney models

Quasiperiodic modulations may be made to the spin-*in*dependent Kronig–Penney model described in section 3.

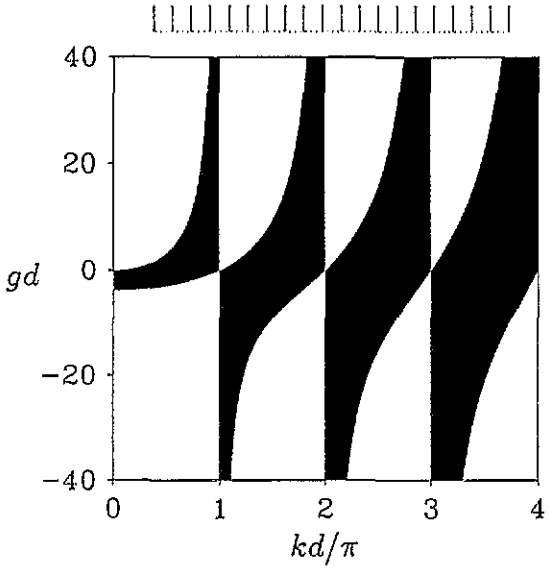

Figure 3. The band structure for the Kronig–Penney model. Gaps are found just above (below) each Brillouin zone boundary for positive (negative) coupling g. A portion of the periodic array of delta function barriers is shown schematically above for comparison with subsequent diagrams.

4.1. FM Kronig–Penney model

Following de Lange and Janssen [26], the spacing between successive delta function barriers may be changed so that the position of the jth barrier is

$$y_j = jd - \Delta d \cos(2\pi j\phi). \tag{13}$$

For rational values of the modulation frequency $\phi = p/q$ (p and q relatively prime), the allowed states may be found using the condition

$$\left|\mathrm{Tr}\left(\prod_{j=1}^{q} \mathbf{m}(k, g, y_j - y_{j-1})\right)\right| \leqslant 2. \tag{14}$$

For $gd = 3\pi/2$, $\Delta d/d = 1/\sqrt{10}$, this structure is shown in figure 4. I call this the 'frequency-modulated (FM) Kronig–Penney model'.

4.2. AM Kronig–Penney model

It is also possible to modulate g sinusoidally while keeping d (the spacing between delta functions) fixed [22]. In this case we have

$$g_j = g_0 + g\cos(2\pi j\phi), \tag{15}$$

and find allowed states when

$$\left|\mathrm{Tr}\left(\prod_{j=1}^{q} \mathbf{m}(k, g_j, d)\right)\right| \leqslant 2. \tag{16}$$

I call this the 'amplitude-modulated (AM) Kronig–Penney model'.

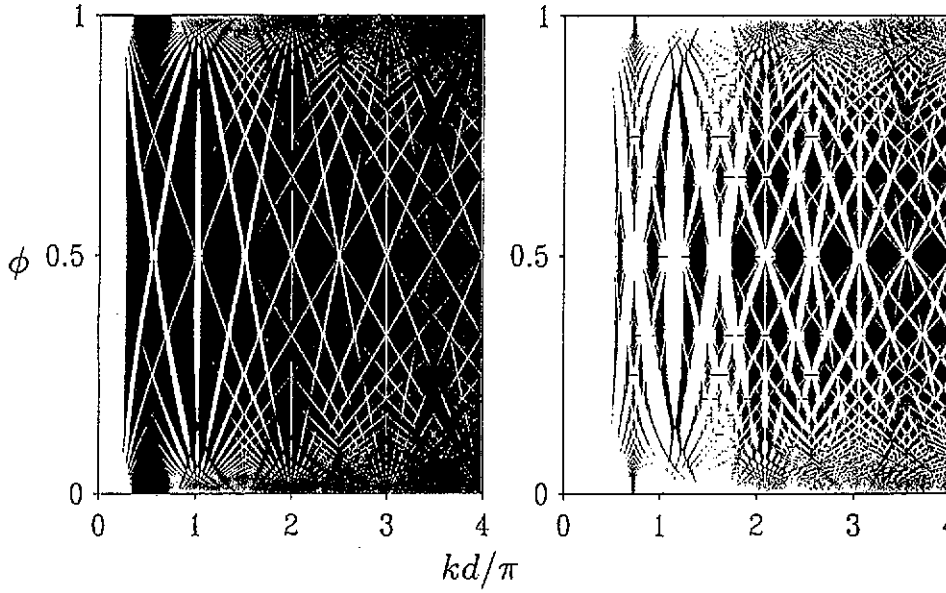

Figure 4. The band structure for the frequency-modulated Kronig–Penney model for $gd = 1$ (left) $gd = 3\pi/2$ (right) and $\Delta d/d = 1/\sqrt{10}$. The frequency-modulated barriers are depicted schematically above; the height (strength) of each barrier remains constant but the distance between barriers is modulated with frequency ϕ.

4.3. Helically modulated Kronig–Penney model

I now introduce a spin-dependent generalization of the Kronig–Penney model which consists of a one-dimensional array of delta function potentials whose strengths depend on the relative orientation of the electron spin and a unit vector located at each delta function whose direction is helically modulated. This corresponds to a one-dimensional *spin-dependent* potential $V(y, \sigma)$ given by

$$V(y, \sigma) = g \sum_{j=-\infty}^{\infty} r_j \cdot \sigma \, \delta(y - jd) \tag{17}$$

where

$$r_j = \begin{pmatrix} \sin(2\pi j\phi) \\ 0 \\ \cos(2\pi j\phi) \end{pmatrix}$$

is a vector which precesses around the y-axis as j increases and σ is the electron spin. I call this the helically modulated (HM) Kronig–Penney model. It is possible to also use a transfer matrix approach to calculate the band structure of this model, but it then becomes necessary to use 4×4 matrices because of the $\sigma \cdot$ dependence of the potential [25]. Therefore, the eigenvalues μ of the transfer matrix in the equation

$$\mathbf{M}(g) \begin{pmatrix} a^{\uparrow} \\ b^{\uparrow} \\ a^{\downarrow} \\ b^{\downarrow} \end{pmatrix} = \mu \begin{pmatrix} a^{\uparrow} \\ b^{\uparrow} \\ a^{\downarrow} \\ b^{\downarrow} \end{pmatrix} \tag{18}$$

must be found, where

$$\mathbf{M}(k,g,d)=\left[\begin{pmatrix}\mathbf{P}(k) & 0\\ 0 & \mathbf{P}(k)\end{pmatrix}\begin{pmatrix}\mathbf{D}(k)^{-1} & 0\\ 0 & \mathbf{D}(k)^{-1}\end{pmatrix}\begin{pmatrix}\cos(\pi\phi)\mathbf{I} & \sin(\pi\phi)\mathbf{I}\\ -\sin(\pi\phi)\mathbf{I} & \cos(\pi\phi)\mathbf{I}\end{pmatrix}\right.$$
$$\left.\times\begin{pmatrix}\mathbf{Q}(g) & 0\\ 0 & \mathbf{Q}(-g)\end{pmatrix}\begin{pmatrix}\mathbf{D}(k) & 0\\ 0 & \mathbf{D}(k)\end{pmatrix}\right]^{q} \tag{19}$$

where

$$\mathbf{I}=\begin{pmatrix}1 & 0\\ 0 & 1\end{pmatrix}\qquad \mathbf{Q}(g)=\begin{pmatrix}1 & 0\\ ig & 0\end{pmatrix}.$$

Hence,

$$\mathbf{M}(k,g,d)=\left[\begin{pmatrix}\cos(\pi\phi)\mathbf{I} & \sin(\pi\phi)\mathbf{I}\\ -\sin(\pi\phi)\mathbf{I} & \cos(\pi\phi)\mathbf{I}\end{pmatrix}\begin{pmatrix}\mathbf{m}(k,g,d) & 0\\ 0 & \mathbf{m}(k,-g,d)\end{pmatrix}\right]^{q}. \tag{20}$$

If ϕ is rational, it is possible to compute the eigenvalues of this matrix to examine whether there are zero, one or two pairs of degenerate eigenmodes. The eigenvalues need to be computed directly since there is no condition on the trace of the transfer matrix analogous to the one used for the modulated spin-independent Kronig–Penney models.

5. Results and discussion

In this section, calculations of the band structure will be presented for both the HM Kronig–Penney model and the AM Kronig–Penney model for different values of the modulation ϕ, and different potential strengths g. The AM Kronig–Penney model is not spin dependent and its potential is the *component* of the HM Kronig–Penney potential *resolved* in the z-direction (i.e., perpendicular to the y-axis). In figure 5, I show the band structure for the AM Kronig–Penney model for modulation $\phi=\frac{1}{2},\frac{1}{3},\frac{1}{4}$, and $\frac{1}{5}$. As q increases ($\phi=p/q$), the unit-cell size grows larger and the band structure splits up into a larger number of sub-bands. This behaviour is as expected from the arguments of section 1, and is of course reminiscent of the fractal nature of the Hofstadter butterfly to which, as argued in section 2, it is strongly related. Each band splits up into q sub-bands, but the gaps between these sub-bands are not always of non-zero width (e.g., the cases of $\phi=\frac{1}{2}$ or $\frac{1}{4}$). The potential for $\phi=\frac{1}{4}$ is the same as that of the $\phi=\frac{1}{2}$ case but the unit-cell size is doubled. Hence the band structure is the same as for the $\phi=\frac{1}{2}$ case, but with half the Brillouin zone size.

For the HM Kronig–Penney model, I will use the following scheme to plot the band structure:

(i) two pairs of allowed eigenmodes: black;
(ii) one pair of allowed eigenmodes: grey;
(iii) no allowed eigenmodes: white.

In figure 6, I plot the band structure for $\phi\simeq 1$. In this case, electrons 'see' a standard spin-independent Kronig–Penney potential, either with positive-strength potentials if the electrons are spin-up, or with negative-strength potentials if the electrons are spin-down. Consequently, the band structure is a superposition of the negative and positive halves of figure 3 (thus the portion shaded grey in figure 6 is a solution for *either* negative *or* positive spin, and the portion shaded black is where the solutions for *both* spin cases overlap). This conclusion can be reached by noting that the transfer matrix (equation (20)) in this case is

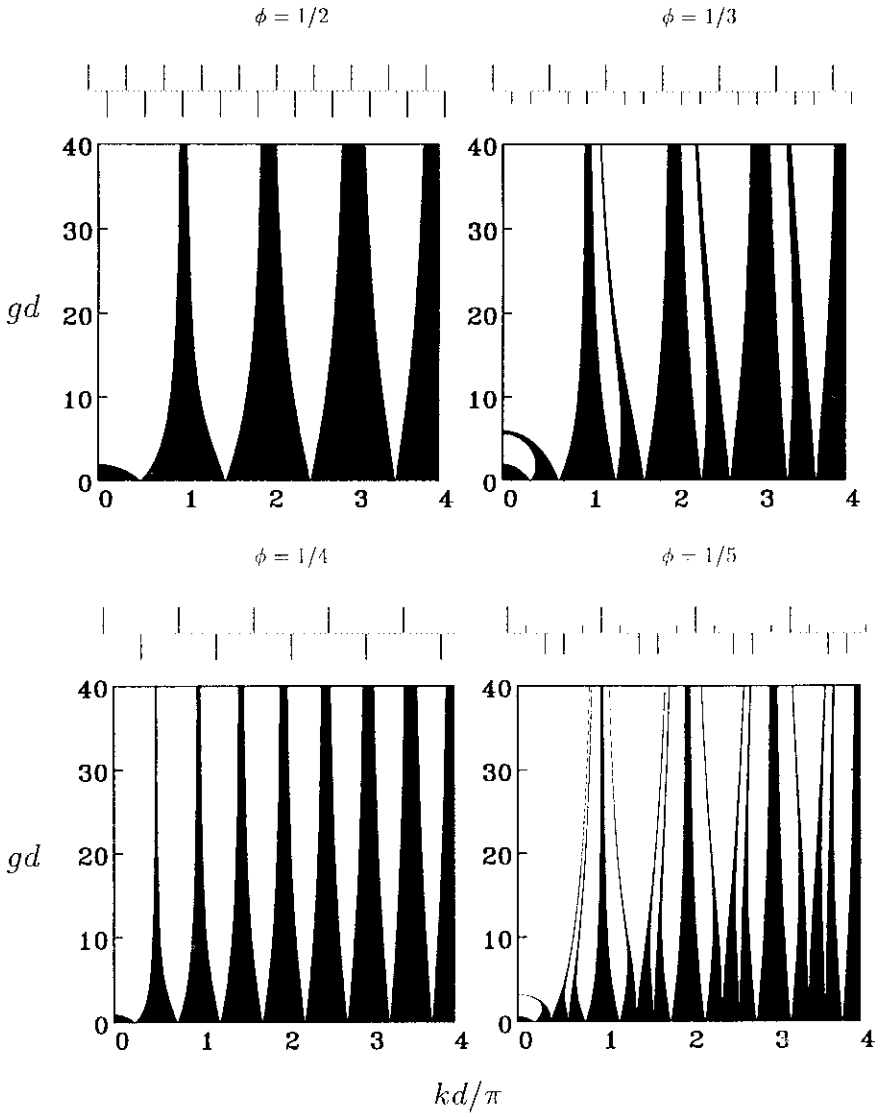

Figure 5. The band structure for the amplitude-modulated Kronig–Penney model for $\phi = 1/2, 1/3, 1/4$ and $1/5$. Above each graph the amplitude-modulated barriers are depicted schematically, the height of each vertical line representing the strength of the delta function potential at that point.

just a block diagonal sum of the transfer matrix for the spin-independent cases for positive- and negative-potential strengths:

$$\mathbf{M}(k, g, d) = \begin{pmatrix} \mathbf{m}(k, g, d) & 0 \\ 0 & \mathbf{m}(k, -g, d) \end{pmatrix}. \tag{21}$$

On the left-hand side of figure 7, I show the band structure for $\phi = \frac{1}{2}$. This is equivalent to the band structure for $\phi = \frac{1}{2}$ in the AM Kronig–Penney model, since electrons see an AM Kronig–Penney potential whether they have spin-up or spin-down. This can be understood

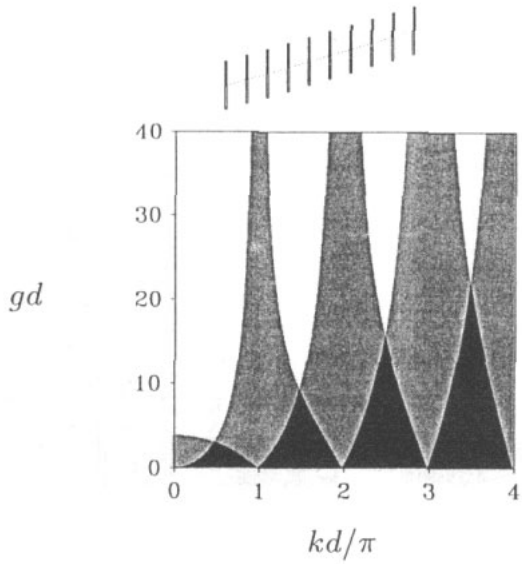

Figure 6. The band structure for the helical Kronig–Penney model for $\phi = 1$. This spin-dependent potential is depicted schematically by an array of barriers which are shaded black and white: depending on the spin of an electron (up=black, down=white for example), the potential consists of an array of positive potentials (barriers) or negative potentials (wells).

by noting that the transfer matrix in this case is given by

$$\mathbf{M}(k,g,d) = -\begin{pmatrix} \mathbf{m}(k,g,d)\,\mathbf{m}(k,-g,d) & 0 \\ 0 & \mathbf{m}(k,-g,d)\,\mathbf{m}(k,g,d) \end{pmatrix} \tag{22}$$

and the set of eigenvalues of this matrix consists simply of two copies of the eigenvalues of $\mathbf{m}(k,g,d)\,\mathbf{m}(k,-g,d)$ and thus leads to allowed states of either spin at precisely the same energies and potential strengths as seen in the AM Kronig–Penney model for $\phi = \frac{1}{2}$. A surprise comes when examining the band structure for other values of ϕ. On the right-hand side of figure 7, I show the band structure for $\phi = \frac{1}{7}$. It is immediately apparent that this has not split up into seven sub-bands. At small coupling g, there are gaps between regions of two pairs of allowed eigenmodes (black) when $kd/\pi = n \pm \phi$ (n an integer). This feature is seen even more strikingly if the dependence of the band structure on ϕ is examined for fixed g (figure 8) for the AM and HM models. For both models, criss-cross gaps are seen at $kd/\pi = n \pm \phi$. In the HM model, the four eigenstates are circularly polarized modes, and when they possess the same spatial rotation as the helical potential, then they can either rotate in the same direction, or in the opposite direction, with differing energy cost. This gives rise to the features at $kd/\pi = n \pm \phi$, where n is an integer. However, one pair of eigenmodes remain allowed except near $\phi = 1/2$ where a gap does open up with increasing coupling g. In the AM model, the criss-cross gaps are repeated recursively, giving rise to a pattern reminiscent of the Hofstadter butterfly to which the model is related [20, 22]. As the coupling strength is increased in both models, the gaps widen—increasingly so at low energy. Yet, the band structure of the HM Kronig–Penney model shows no fractal nature, in contrast to the AM case, in which a great deal of fine structure is observed. This is due to the fact that the latter model, together with the FM model of section 4.3, breaks the translational symmetry of the unmodulated lattice, by increasing the size of the unit cell by a factor of q (where $\phi = p/q$). In the HM model, although the translational symmetry of

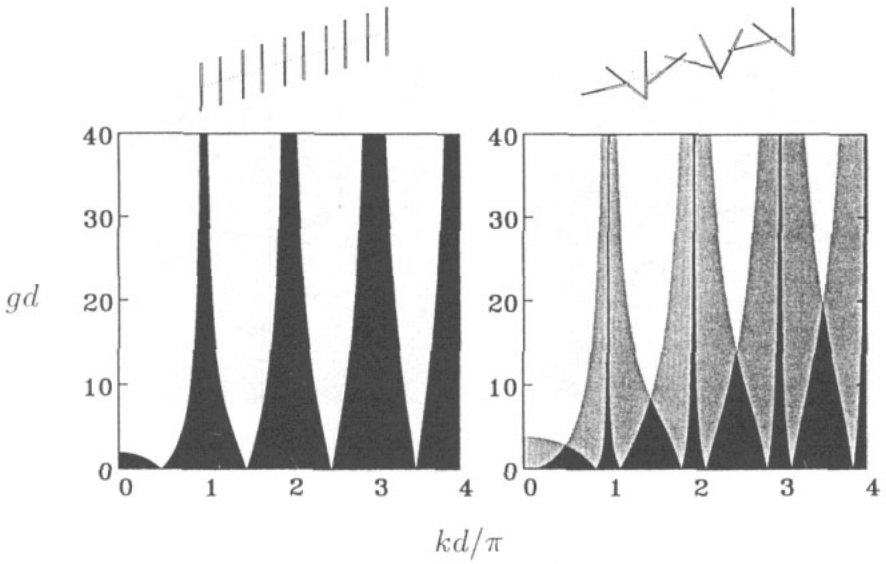

Figure 7. The helical Kronig–Penney model for $\phi = 1/2$ and $\phi = 1/7$. The spin-dependent potentials are illustrated in each case using the scheme of figure 6: for $\phi = 1/2$, an electron is in a potential which is alternately positive and negative; for $\phi = 1/7$, the axis of quantization rotates with a period of seven delta functions. The exact potential experienced by each electron depends on its spin.

the unmodulated lattice is broken by the modulation, the operation of translation by d and rotation by $2\pi\phi$ is a symmetry operation which commutes with the Hamiltonian, and so an equivalent Bloch theorem can be derived in terms of this operation. A transfer matrix, operating over only one delta function period, can be derived independently of q with no restriction to rational ϕ, since the exponent q in equation (20) is superfluous (if a transfer matrix $\mathbf{A}^q$ has m eigenvalues with unit modulus, so does the matrix $\mathbf{A}$). Thus the fractal structure is 'quenched' by the symmetry in this case; despite the geometric quasiperiodicity of the potential which in the spin-independent case produces a band structure which is related to the Hofstadter butterfly (a fractal), the higher symmetry of the spin-dependent case is sufficient to remove that structure completely.

This can be clearly seen in figure 9 where the circle formed by the projection onto the x–z plane of the the helical path along which the magnetization vector precesses is squashed into an ellipse, and finally a line (representing the spin-dependent version of the amplitude-modulated model). In this case, the vector in the spin-dependent potential (equation (17)) is given by

$$r_j = \begin{pmatrix} \beta \sin(2\pi j\phi) \\ 0 \\ \cos(2\pi j\phi) \end{pmatrix}$$

where the parameter β is the ratio of the minor and major axes of the ellipse. This is illustrated in figure 9 for the modulation $\phi = \frac{1}{5}$. The symmetry of the helical (circle) system is reflected by the absence of many gaps, but as the circle is squashed into an ellipse, the gaps appear, increasing in size until they are visibly present at all values of the barrier potential strength.

It is also possible to study a model in which the magnetization vector precesses around the surface of a cone (in the manner of a spin wave), and in this case, the fractal spectrum

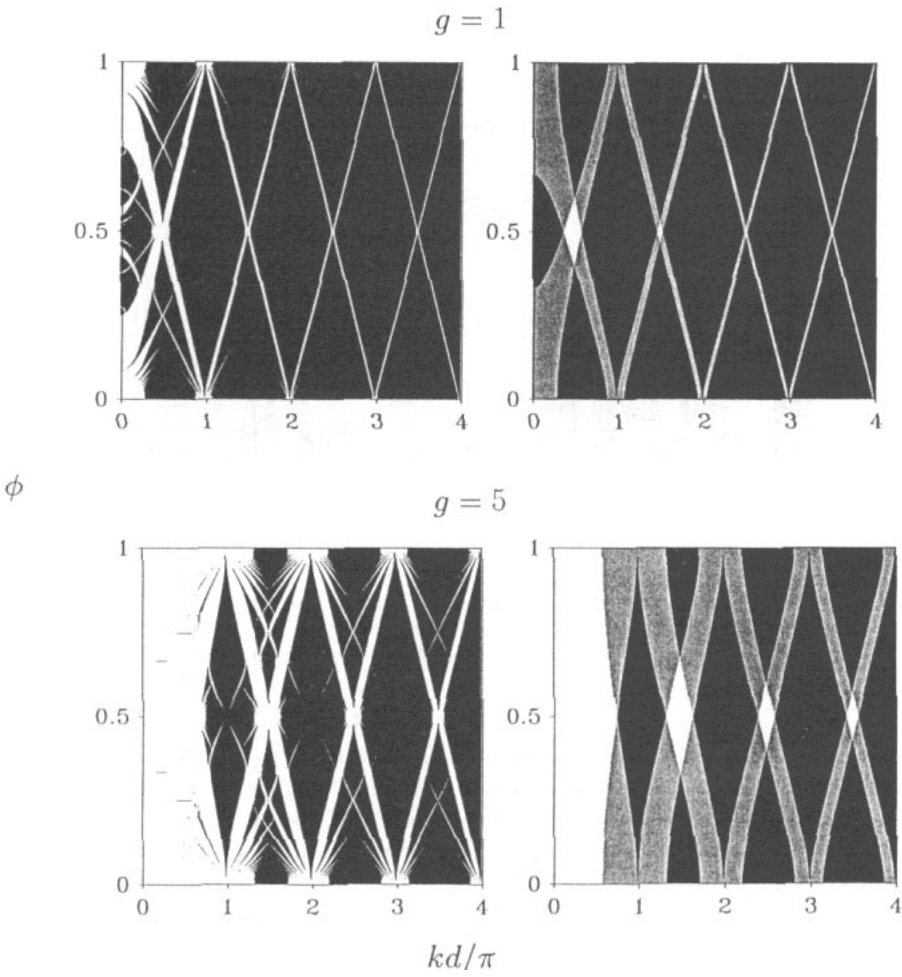

Figure 8. The band structure for the AM (left) and HM (right) Kronig–Penney models for $g = 1$ (top) and $g = 5$ (bottom).

is also quenched for precisely the same reason as it is in the helically modulated model. Using this method, it is therefore possible to reproduce the abundant range of magnetic structures observed in rare-earth magnetic systems and systematically to examine their band structure, albeit in a simplified one-dimensional model.

6. Summary

A transfer matrix method has been used to calculate the band structure of a spin-dependent generalization of the Kronig–Penney model. This consists of a one-dimensional array of delta function potentials whose strengths depend on the relative orientation of the electron spin and a vector located at each delta function site; the direction of the vector can be helically modulated. The HM Kronig–Penney model has been compared with the AM Kronig–Penney model in which the strengths of each delta function potential are modulated independently of the electron spin. The most important result of this study is that although

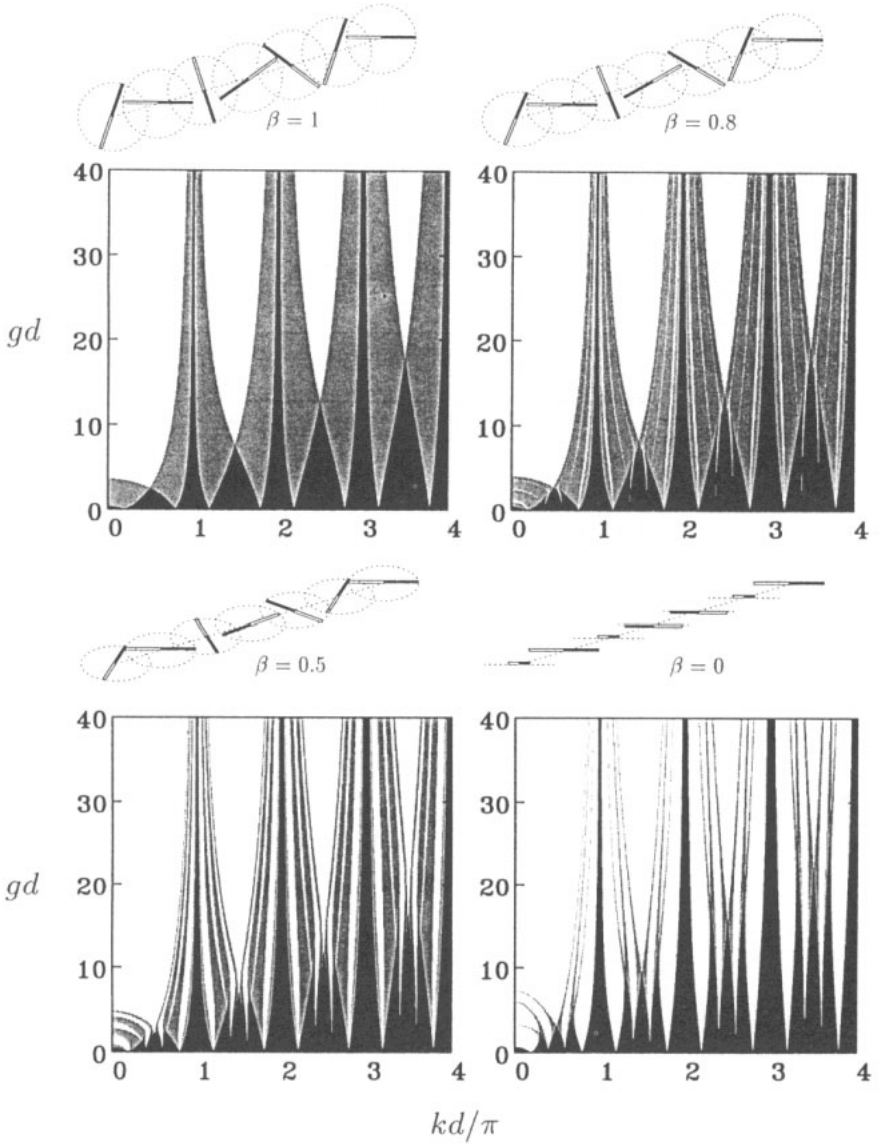

Figure 9. The quenching of the fractal structure for $\phi = 1/5$. The spin-dependent potentials lie on a helical structure in which the circle, which is traced out by the projection of the helical path on a plane perpendicular to the axis of the helix, becomes elliptical with minor/major axis ratio β and hence is progressively squashed into a line as β runs from 1 to 0.

the potential of the HM model may not possess translational symmetry if the helical modulation frequency is irrational, a combination of a rotation and a translation can commute with the Hamiltonian so that the fractal structure observed in the AM Kronig–Penney model is quenched.

Acknowledgments

I am grateful to the EPSRC for the award of a research fellowship and to K M Blundell, A J Fisher, A J Schofield and J Singleton for useful discussions.

References

[1] Shechtman D, Blech I, Gratias D and Cahn J W 1984 *Phys. Rev. Lett.* **53** 1951
[2] Steinhardt P J and Ostlund S 1987 *The Physics of Quasicrystals* (Singapore: World Scientific)
[3] Kohmoto M, Kadanoff L P and Tang C 1983 *Phys. Rev. Lett.* **50** 1870
[4] Kohmoto M 1983 *Phys. Rev. Lett.* **51** 1198
[5] Kohmoto M, Sutherland B and Tang C 1987 *Phys. Rev.* B **35** 1020
[6] Avishai Y and Berend D 1991 *Phys. Rev.* B **43** 6873
[7] Merlin R, Bajema K, Clarke R, Juang F Y and Bhattacharya P K 1985 *Phys. Rev. Lett.* **55** 1768
[8] Toet D, Potemski M, Wang Y Y, Maan J C, Tapfer L and Ploog K 1991 *Phys. Rev. Lett.* **66** 2128
[9] Solokoff J B 1985 *Phys. Rep.* **126** 189
[10] Luck J M 1989 *Phys. Rev.* B **39** 5834
[11] Janner A and Janssen T 1977 *Phys. Rev.* B **15** 643
[12] Batalla E, Rasavi F S and Datars W R 1982 *Phys. Rev.* B **25** 2109
[13] Coleman L B, Cohen M J, Sandman D J, Yamagishi F G, Garito A F and Heeger A J 1973 *Solid State Commun.* **12** 1125
[14] Lovesey S W 1988 *J. Phys. C: Solid State Phys.* **21** 2805, 4967
[15] Brackstone M A and Lovesey S W 1989 *J. Phys.: Condens. Matter* **1** 6793
[16] Simon B 1982 *Adv. Appl. Math.* **3** 463
[17] Matthews J and Walker R L 1970 *Mathematical Methods of Physics* 2nd edn (New York: Addison-Wesley) p 198
[18] Aubry S and Andre G 1980 *Ann. Israel Phys. Soc.* **3** 133
[19] Harper P G 1955 *Proc. Phys. Soc.* A **68** 874
[20] Hofstadter D R 1976 *Phys. Rev.* B **14** 2239
[21] Guillement J P, Helffer B and Treton P 1989 *J. Physique* **50** 2019
[22] Bellisard J, Formoso A, Lima R and Testard D 1982 *Phys. Rev.* B **26** 3024
[23] Walker J S and Gathright J 1994 *Am. J. Phys.* **62** 408
[24] Odagaki T and Aoyama H 1989 *Phys. Rev.* B **39** 475
[25] Blundell S J and Bland J A C 1992 *Phys. Rev.* B **46** 3391
[26] de Lange C and Janssen T 1983 *Phys. Rev.* B **28** 195